International Journal of Engineering and Geosciences
https://dergipark.org.tr/en/pub/ijeg
e-ISSN 2548-0960

An unmanned aerial vehicle based investigation of roof patch suitability for solar panel installation

Nizar Polat [*1], **Abdulkadir Memduhoğlu** [1]

[1] *Harran University, Department of Geomatic Engineering, Türkiye, nizarpolat@harran.edu.tr, akadirm@harran.edu.tr*

Cite this study: Polat, N., & Memduhoğlu, A. (2024). An unmanned aerial vehicle based investigation of roof patch suitability for solar panel installation. International Journal of Engineering and Geosciences, 9 (2), 281-291

https://doi.org/10.26833/ijeg.1424400

Keywords
Solar radiation potential
Unmanned aerial vehicle
GIS
Image processing

Research Article

Received: 23.01.2024
Revised: 12.03.2024
Accepted: 17.03.2024
Published: 25.07.2024

Abstract

This study presents a Geographic Information Systems (GIS) and Unmanned Aerial Vehicle (UAV) based approach to determine suitable roof patches of buildings for solar panel installation in Harran University (Şanlıurfa) campus area. Initially, the Solar Radiation Potential (SRP) of the study area was calculated using a UAV-based Digital Surface Model (DSM) in GIS. Then, a correction process was applied to this theoretically calculated SRP by using an adjustment coefficient derived from 5-year measurements of the Solar Power Plant (SPP) located in the region. This coefficient was used to adjust the calculated SRP and compared with the SPP measurements at a concurrent period. The rooftop objects were segmented by textural analysis to determine the suitable panel installation patches on the buildings. Then, the obtained suitable patches are divided into four different classes considering the adjusted total SRP to find panel installation priority. Finally, the calculated electricity potential of the suitable roof patches could meet approximately 65% of the yearly consumption of campus buildings. This paper reveals that in GIS-based SRP studies, it is necessary to detect the rooftop objects to obtain the solar panel installation area more accurately, and a correction should be applied to approximate the theoretically calculated SRP values to the actual values.

1. Introduction

In today's world, energy usage is perceived as an indicator of technological development and high welfare levels for developed countries. All fundamental and essential aspects of life, such as industry, trade, housing and transportation, depend on energy. However, the primary energy resources of the world such as water and fossil-based fuels, are in continual depletion. This depletion affects human life as well as energy production directly. Moreover, the usage of these primary energy resources causes ecological damages such as drought, air and soil pollution, etc. This has driven many countries to use clean and renewable energy sources such as wind, geothermal and solar [1]. In the past few decades, these alternative renewable energy resources made a rapid change, especially in rural settlements [2]. According to Elliot et al. [3], any kind of renewable energy source provides opportunities for electricity generation at a public service scale, village and farm needs, and off-grid independent energy generation. At this point, some parameters such as energy demand, environmental conditions and especially power station locations should be considered to establish alternative power systems [4]. In this context, solar energy has the potential to become more popular than other renewable energy sources with its accessibility, economic advantage, and ease of use.

Estimating solar energy is a valuable tool for developing energy strategies, designing facilities and urban planning [5-9]. As it is known the fundamental consideration for solar energy is to detect Solar Radiation Potential (SRP) both spatially and temporally. This potential can obtain either meteorology station measurements (used to estimate the solar radiation through interpolation in the areas) or Geographic Information Systems (GIS) based Digital Surface Model (DSM) approach [10]. A meteorological station based study was performed by Nematollahi and Kim [11]. They calculated the yearly horizontal radiation of 24 meteorology stations for five years to get a feasibility report for new Solar Power Plants (SPP). Meteorology stations may not always be used for several reasons such as inconvenient location, insufficient station number, incompatible technology and missing parameters [12].

Due to the scarcity of meteorology stations, GIS-based studies are more abundant in scientific literature. In these kinds of studies, DSM is an essential input for the SRP calculation based on the hemispherical model. The spatial resolution of the DSM is important and depends on the generation methods. For instance, while a DSM (~1 m) generated with Light Detection and Ranging (LiDAR) data may be sufficient to get the slope and orientation of rooftops in terms of spatial resolution, a Shuttle Radar Topography Mission (SRTM) elevation data (~30 m) could not be used for this purpose. Therefore, high resolution data is required for solar panel installation studies.

The roof of a building is the most suitable patch for solar panel installation. Thus, SRP calculation becomes more complicated due to the requirement for comprehensive knowledge of the geometric and physical conditions of rooftop structures [13]. Generally, in city-scale studies, a LiDAR-based DSM is used to calculate the SRP of the entire city surface. Subsequently, the building footprints and directions are used as constraints to obtain rooftop SRP values [14]. Kucuksari et al. [15] followed a similar procedure and used airborne LiDAR data with GIS in a campus area to calculate SRP using slope, aspect, elevation and insolation as input parameters. Then, to get the long-term net profit of rooftop solar panel installations, electricity potential was examined in consideration of possible costs. Huang et al. [14] proposed a Graphical Processing Unit-based SRP calculation model with LiDAR data using GIS. The suitable roofs were decided according to the yearly average total radiation, slope, and aspect. Verso et al. [16] applied a multi-criteria approach based on GIS and DSM to calculate the SRP. Then several criteria were applied such as building shapes, types, annual solar potential and panel size to detect suitable roofs.

Determining the appropriate roof patches and evaluating their SRP is important for solar panel installation [15]. Depending on the complexity of the urban area, the accuracy and resolution of the spatial data may vary. The high-resolution DSM can be obtained by satellite imagery and laser systems, but it is not efficient in terms of economy, time, and updating. In this context, DSMs with different spatial accuracy and resolution can be produced using Structure-from-Motion (SfM) based Unmanned Aerial Vehicle (UAV) photogrammetry. This approach, which has been used extensively in the last two decades, brings great advantages. It provides cheaper and higher spatial resolution DSM in comparison with LiDAR, especially for local city areas [17].

Compared to conventional manned aerial photogrammetry, UAV photogrammetry has serious advantages in areas such as flight altitude, cost, time, repetitive use, and image processing [18]. It is also suitable for photogrammetric flights. Especially the SfM approach used in the processing of aerial photographs obtained by UAV gives very successful results. This approach is an innovative, user beneficial and low-cost photogrammetric technique, which has been used widely over the last few years [19].

Besides, the possibility of re-use of UAV systems, being automatic, portable, and easy to use in the urban area makes it more advantageous [20]. Thus, UAV-based DSMs can be used in SRP studies for urban areas. In this regard, Shao et al. [21] applied a UAV-based procedure to get high resolution data on roofs. They classified the building types and building roofs (flat, non-flat) to make a better decision for panel installation. Dewanto et al. [22], calculated rooftop SRP from UAV-based DSM and overlaid it on a three-dimensional (3D) model of campus buildings using a web-based GIS environment. Fuentes et al. [23], calculated the SRP of an individual building roof with UAV-based DSM. After solar panel installation, the generated electricity production was compared with the calculated potential for a year.

There are two common gaps in the mentioned SRP studies: (1) the rooftop objects were not considered and (2) the SRP is based on theoretical calculations. Generally, in GIS-based studies, the entire rooftop is considered a potential solar panel installation area. However, this assumption may deviate considerably in the real world, especially in cases of different roof types (flat, non-flat). Moreover, rooftops may be occupied by different objects such as chimneys, air conditioners, ventilation, antennas, or solar water heating panels. In such cases, a detailed analysis of the rooftop is required to calculate accurate SRP. For this analysis, an high-resolution DSM (e.g., pixel < 25 cm) is needed. Thus, rooftop objects can be eliminated and the most suitable areas for solar panel installation can be determined by segmenting roofs in more detail. Although in some studies segmentation is used to detect the roof planes, the rooftop objects on the segmented planes were ignored. Furthermore, SRP calculation performed in hemispherical based GIS software gives approximate results since it does not contain real meteorological factors. This situation causes the calculated SRP to be different from the actual Solar Radiation (SR). While a comparison between generated electricity and GIS-based calculated energy was performed in some studies, no adjustment process mentioned calculated SRP.

The objectives of this study are twofold: first, it attempts to determine the most suitable roof patches for solar panel installation; second, it attempts to adjust the calculated SRP. For this purpose, a textural analysis was performed using high-resolution DSM to detect the rooftop objects. Then, monthly, seasonal and annual coefficients were calculated with the data (for 5 years) obtained from the SPP in the study area and the most suitable coefficient was used to adjust the calculated SRP.

2. Method

The study was held in the Harran University Osmanbey Campus located in Şanlıurfa which is in southeast Turkey (Figure 1). The annual average (last 30 years) of the sunshine duration of the city is over 8.5 h/d [24]. According to the long-term average of SR reported in Global Solar Atlas [25], Şanlıurfa has one of the highest SRP in the country.

The SR of a particular point on the earth depends on the orientation and elevation [26]. Thus, the SRP of that point is mainly calculated according to the hemispherical

viewshed algorithm. A DSM can supply necessary information about the surrounding topography including the obstacle and shadow area of that point [27]. Although DSM is sufficient for SRP calculation, various parameters such as meteorological station data [14], classified satellite images [28] and topographic maps [29] can be used as inputs depending on the purpose of the study. In our case, the building footprints, SPP measurements and UAV based DSM were used as input. The workflow of the study is given in Figure 2.

In the study, a workflow including photogrammetric UAV flight, SfM, textural analysis and GIS based SRP calculation was carried out. There are several important and specific steps within this workflow. First, the high-resolution DSM of the region was produced using SfM-based UAV photogrammetry. Second, textural analysis was performed on high resolution DSM to detect rooftop objects. Third, is the coefficient calculation for the SRP adjustment. Finally, the electricity potential was calculated according to the suitable roof patches and was compared with the actual consumption.

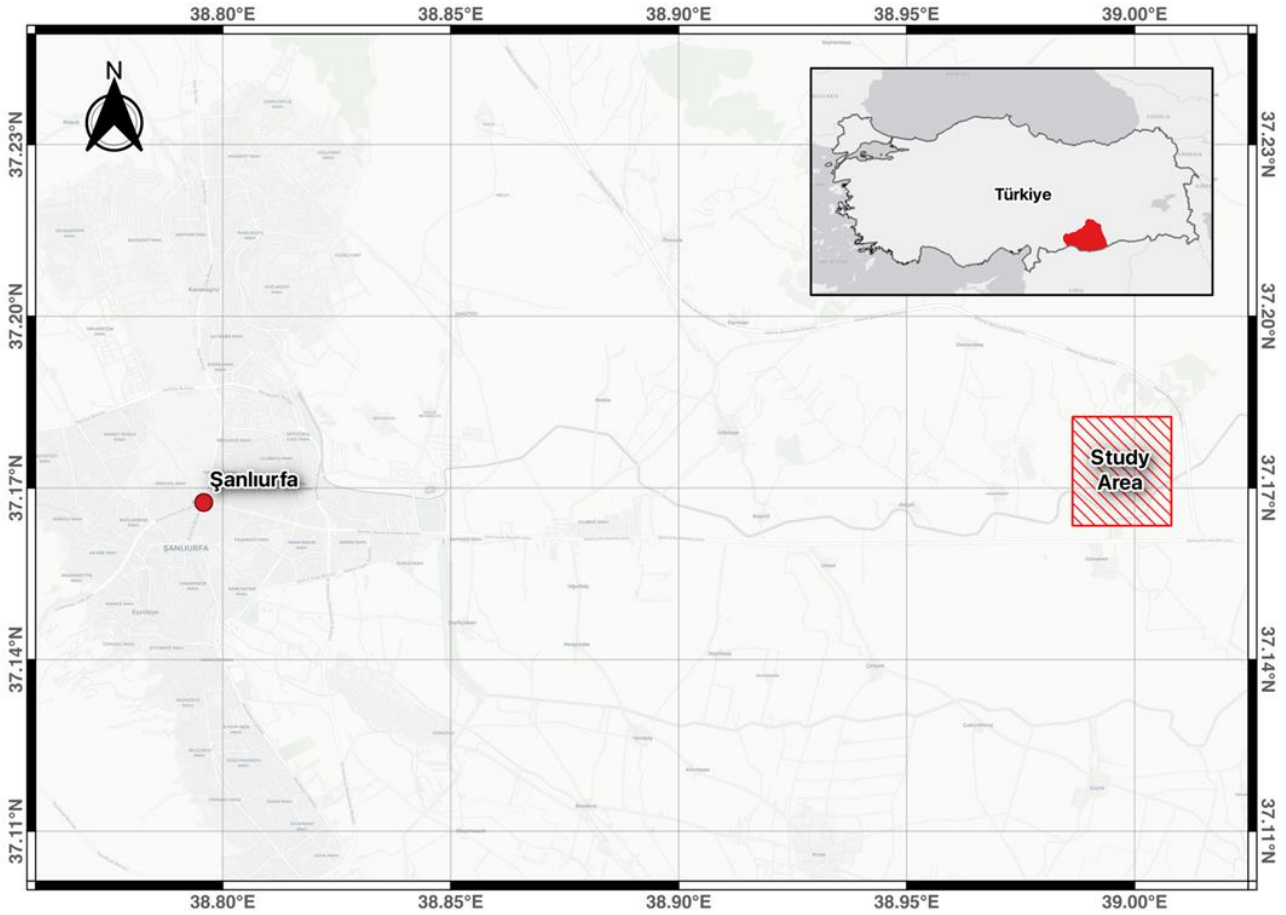

Figure 1. The study area.

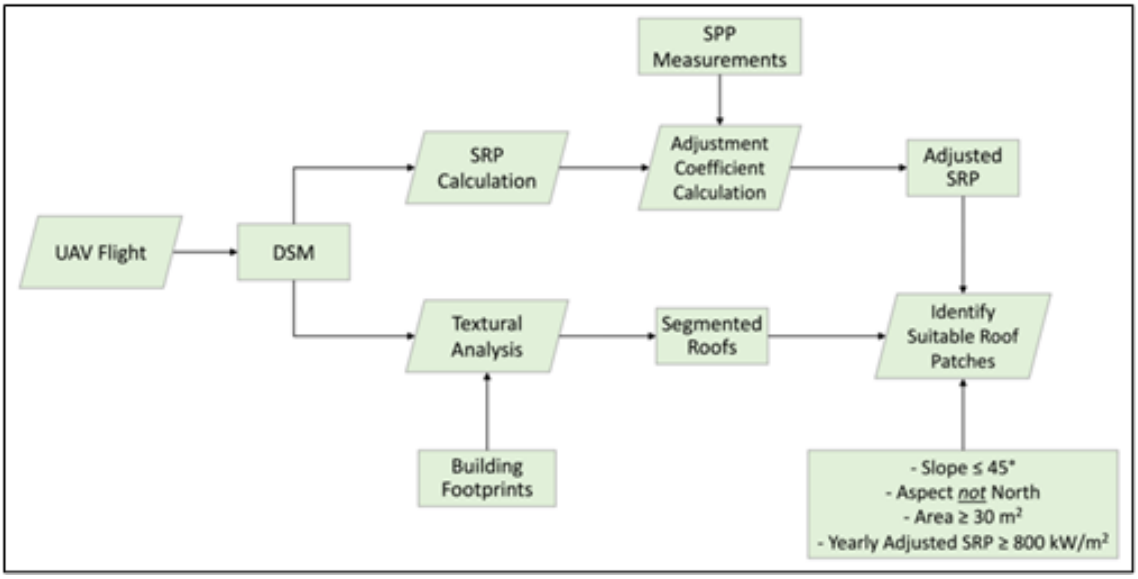

Figure 2. The workflow of the study.

2.1. UAV photogrammetry

There are some differences between SfM and traditional photogrammetry in terms of mathematical and statistical approaches. Traditional photogrammetry looks for solutions by using global consistency, compatibility, the accuracy of measurements and model validity. On the other hand, SfM is an image matching technique that generates a 3D model of an object by automatically aligning positions, camera parameters and 3D geometry of the object with an appropriate overlap rate through a photogrammetric approach [30]. Then, a photogrammetric bundle block adjustment is used to build a local model with all generated 3D points. Today, several SfM-based image processing software can generate high resolution DSM and orthophoto from aerial images captured with UAV platforms [20]. Lucieer et al. [31] managed to generate a 2 cm resolution DSM to get microtopography with Agisoft software. Toprak et al. [18] reached under cm accuracy in a rocky archeological site with the SfM approach. Besides, due to the high spatial resolution data of UAV systems, they can be used in biomass estimation and yield prediction [32], cotton plant height [33] and accurate extraction of buildings in a complex urban area [34].

2.2. Textural analysis

The purpose of texture analysis is to identify flat areas suitable for panel installation. At this point, texture analysis aims to detect objects that disrupt the flatness of a roof section and could obstruct panel installation, such as air conditioning units, antennas, or chimneys.

Images are generally described with color values, brightness and pixel size. On the other hand, texture parameters such as variance, dissimilarity and entropy are rarely used. A pixel of an image can contain color and brightness values. However, the texture becomes meaningful with a set of neighboring pixels. Mathematically, the Gray Level Co-Occurrence Matrix (GLCM) is used to get a two-dimensional histogram of the gray levels of a neighboring pixel pair. In other words, GLCM displays the frequency of pixel pair apparency in an image. GLCM is used to calculate texture parameters which are suggested by Haralick et al. [35]. In this study, the GLCM-based variance parameter was used to detect rooftop object segments. Briefly, variance defines the heterogeneity of pixel neighboring. Equation 1 is used to calculate the variance parameter.

$$\sum_{i=0}^{N_g-1} (i-M)^2 P(i) \quad (1)$$

where:

- P(i) denotes pixel probability.
- Ng refers to pixels' gray value.
- M is the mean pixel value obtained from input DSM.

2.3. GIS-based calculation of solar radiation potential

It is a fact that the amount of SR emitted from the sun is different from the amount reaching the earth's surface by passing through the atmosphere. Ŝúri and Hofierka [36] reported three main elements that affect SR: Earth's position, Earth's topography, and atmospheric conditions. In a GIS-based SRP calculation, above mentioned elements are used as solar parameters, DSM and atmospheric conditions (absorption and dispersion) respectively. DSM is used to determine the maximum possible obstruction angle in consideration of all directions around the geographical location of the study area [27]. The detected angles allow us to get a hemispherical viewshed that consists of both visible and blocked directions in the sky [26]. This sky map is used to calculate the diffuse SR (caused by the scattering of sunlight in the atmosphere) received at a particular location in DSM. Then, the sun map is produced according to the position change of the sun over time (hour, day and month) considering the position of the study area. The sun map is used to estimate the amount of direct SR received by a particular location in DSM [37].

The generated viewshed, sun map, and sky map are used to calculate direct and diffuse SR for every single pixel of DSM in GIS [38]. The whole amount of SRP which is called the global SR ($Global_T$) is derived from the sum of the total direct SR (Dir_T) and total diffuse SR (Dif_T) (Equation 2) [39].

$$Global_T = Dir_T + Dif_T \quad (2)$$

The total direct SR (Dir_T) of a particular location on the earth's surface is the sum of the direct SR from all directions of the sun map (Equation 3) [27].

$$Dir_T = \sum S_{Const} * \beta^{m(\theta)} * SunDur_{\theta,\alpha} * SunGap_{\theta,\alpha} * \cos(Angln_{\theta,\alpha}) \quad (3)$$

where:

- θ – with a centroid at a zenith angle.
- α – azimuth angle.
- S_{Const} — The solar flux constant (1367 W/m²) [40].
- β —The atmosphere transmissivity for the shortest path in the zenith direction.
- $m(\theta)$ — The relative optical path length.
- $SunDur_{\theta,\alpha}$ — The time duration of the sky map.
- $SunGap_{\theta,\alpha}$ — The gap fraction for the sun map.
- $Angln_{\theta,\alpha}$ — The angle of incidence between the axis normal to the surface and the centroid of the sky sector (tilt angle).

Diffuse radiation (Dif_T) is calculated using Equation (4) [27]:

$$Dif_T = R_{glb} * P_{dif} * Dur * SkyGap_{\theta,\alpha} * Weight_{\theta,\alpha} * \cos(Angln_{\theta,\alpha}) \quad (4)$$

where:

- θ – with a centroid at a zenith angle.
- α – azimuth angle.
- R_{glb} — The global normal solar radiation.
- P_{dif} — The proportion of global normal radiation flux that is diffused. It is approximately 0.2 for very clear sky conditions and 0.7 for very cloudy sky conditions.
- Dur — The time interval for analysis.
- $SkyGap_{\theta,\alpha}$ — The gap fraction for the sky map.
- $Weight_{\theta,\alpha}$— The proportion of diffuse radiation originating in each sky sector relative to all directions.
- $Angln_{\theta,\alpha}$— The angle of incidence between the intercepting surface and the centroid of the sky sector (tilt angle).

In equations for both diffuse (3) and direct solar radiation (4), the variables θ, α and $Angln_{\theta,\alpha}$ —which represent the zenith, azimuth, and tilt angles, respectively—are dependent on the Earth's position and vary over time. Latitude plays a significant role in solar geometry, influencing these parameters in relation to the sun's position.

2.4. Estimation of adjustment coefficient

As mentioned in Section 1, GIS-based calculated SRP varies from actual SR. Thus, an adjustment process is needed. For this purpose, monthly average SR data for 6 years were obtained from the SPP located in the study area. 5-years of SR data (2015-2020) were used for the Adjustment Coefficient (AC) estimation and the remaining 1-year (2021) SR data were used for control purposes. The 5-year SR data were grouped into time intervals as monthly, seasonal and yearly and their averages were obtained. Similarly, the calculated SRP data for 2021 were grouped as monthly, seasonal and yearly. The 5-year average of SR values was proportioned to the 2021 calculated SRP values and then monthly, seasonal and annual coefficients were calculated. In the end, 3 different types (monthly, seasonal and annual) of ACs were obtained by using Equation 5.

$$AC_t = \frac{\left(\sum_{i=2015}^{2020} SR_{t_i}\right)/5}{SRP_{2021_t}} \quad (5)$$

where:

- AC is the Adjustment Coefficient.
- t – is the time interval (e.g., January for monthly, Spring for seasonal and year for annual adjustment calculation $t = i$).
- i – is the measured year of the SPP data.
- SR – is the solar radiation value of the corresponding year.
- SRP – is the calculated solar radiation potential from GIS.

By applying these ACs to 2021 calculated SRP, monthly, seasonal and annually corrected SRP values were obtained. The corrected SRP values were compared with 1-year (2021) of measured SR data to determine the most suitable AC. Thus, the GIS-based calculated SRP values are approximate to the real values by using the most suitable AC.

For AC calculation, it is necessary to have a monthly average SR measurement collected from near the region of interest. Since meteorological conditions directly affect the sunshine duration during the day, hourly SR measurements must be obtained for a reliable monthly average SR measurement. In addition, the location of the study area directly affects the SR value. Any significant changes in these parameters will require a recalculation of AC.

2.5. Identifying suitable roof patches

All the roof patches of a building cannot be suitable for solar panel installation due to the above-mentioned rooftop objects. Thus, all roof patches were determined as suggested in Section 2.2. Consequently, rooftop objects were detected, and several parameters were used to identify suitable roof patches.

The first parameter is the minimum installation area. This parameter should be decided according to the solar panel dimensions and orientations to be installed. That means this parameter may vary depending on the project requirements, panel and building type. Although Khanna [41] reported that less than 30 m^2 of building roof patches may not be suitable for panel installation, Palmer et al. [42] used 8 m^2 for houses and Huang et al. [14] used 10 m^2 for urban buildings. We used this value as 30 m^2 in consideration of large faculty buildings and panel dimensions. The second parameter is the slope. It is not feasible to install panels over a 45-degree slope. So, a lower than 45-degree slope is used as a parameter in this study. The third parameter is the aspect. The study area is located in the northern hemisphere. Therefore, the amount of SRP is inadequate for the north facing roof patches. So, these patches were removed. The last parameter is the minimum amount of the yearly average SRP of the patches. This parameter was used as a yearly minimum of 800 kWh/m^2.

2.6. Estimation of electricity potential

Spatial variations of solar panel installations on the roof are critical to understanding the SRP [43]. Calculating the electricity potential from SRP depends on the installation scenarios of the panels and the panel properties [44]. In this context, tilt and panel area affect the total number of panels, while efficiency and performance ratio values affect the total electricity potential. For this reason, creating building-based scenarios may give more accurate results. However, this approach is not effective in urban areas with many buildings. Additionally, there is no need for spaces and access roads between the solar panels on a roof, unlike

the solar panels installed in the open area according to an expert opinion from the SPP. Therefore, in our case, it has been assumed that all suitable roof patches are installed with similar solar panels (25% tilt and 1.67 m^2 panel area) of SPP in the region. Hence, the same panel parameters namely efficiency and performance ratio values were used for electricity potential calculation. To determine electricity potential Equation 6 was used [13].

In this study, the SR value refers to the adjusted SRP (kWh/m^2), the efficiency of the solar panel is 16% and the performance ratio of the solar panel is 88%. The efficiency and performance ratio of the panel were obtained from the manufacturer of the panels.

$$Electricity\ Potential = SR\ value \times Efficiency \times Performance\ Ratio \quad (6)$$

3. Results and discussion

In the study, ten different photogrammetric flight plans were prepared, and UAV (DJI Mavic 2 Pro) flights were performed to create a high-resolution DSM. For the flight parameters, the elevation was decided as 100 m for 70% overlaps both forward and literal. 1019 suitable aerial images were captured for the 4.16 km^2 area. The calculated ground sample distance was 3.7 cm. In the end, the orthophoto and a 25 cm spatial resolution DSM were generated for the study area (Figure 3). All photogrammetric products were generated in Pix4D software.

Before textural analysis, the DSM was masked with building footprints. Then the texture-based variance parameter was generated by using masked DSM and the segments of the rooftop objects were obtained. Sample buildings with original and segmented footprints are given in Figure 4.

As seen in Figure 4, the rooftop objects such as air conditioner parts, antenna, chimney and elevator room were detected successfully. Thus, 147 parts of the original building footprints were segmented into 699 parts. This situation allows us to investigate all segmented roof patches in detail for panel installation.

Figure 3. Orthophoto and DSM of the study area.

Figure 4. Sample buildings with original and segmented footprints.

After the rooftop segmentation, comparison and adjustment were performed between calculated SRP and SPP measurements. To find a suitable AC, three different SR data were used (Table 1). The first one is the calculated SRP of the study area from March 2021 to February 2022. Second is the monthly measurements of the SPP for a continuous period of 5 years from March 2015 to February 2020. This data was used to calculate ACs. The third one is the SPP measurement from March 2021 to February 2022. This data was used to compare adjusted SRP values.

In Table 1, the total of the 1-year SPP measurements (2021-2022) is close to the total of the 5-year SPP measurements (2015-2020). However, the total of the

calculated 1-year SRP (2021-2022) significantly differs from these measurements. Therefore, the 5-year SPP measurements were compared with calculated SRP utilizing monthly, seasonal and annual periods. According to this comparison, three types of ACs were calculated regarding Equation 5 (Table 2).

Table 1. Monthly averages of solar radiation values (kWh/m²).

Month	Calculated SRP (2021-2022)	SPP Meas. (2015-2020)	SPP Meas. (2021-2022)
March	105.13	141.24	123.47
April	139.86	181.14	158.52
May	172.32	211.36	218.13
June	176.11	239.88	219.35
July	178.44	248.62	236.21
August	156.46	219.42	225.46
September	116.07	176.70	208.40
October	79.35	127.97	152.70
November	47.08	85.98	130.99
December	33.96	65.41	72.23
January	43.12	71.49	91.25
February	63.47	92.18	97.96
Total	1311.37	1861.37	1934.66

Table 2. Calculated Acs.

Month	Adjustment Coefficients		
	Monthly	Seasonal	Annual
March	1.343		
April	1.295	1.288	
May	1.227		
June	1.362		
July	1.393	1.386	
August	1.402		1.502
September	1.522		
October	1.613	1.654	
November	1.826		
December	1.926		
January	1.658	1.679	
February	1.452		

The calculated coefficients were used to adjust the SRP values. In order to examine the effects of the coefficients, the calculated and adjusted SRP values for 2021-2022 were compared with SPP measurements for 2021-2022 (Figure 5).

Although there is not a big difference in trend (similar fluctuation) between the SPP measurement (turquoise) and the calculated SRP (blue), there is a considerable difference in quantity. The main reason for this is the lack of meteorological models in GIS-based approach. The theoretical values are approximated to the actual values with the calculated ACs. As seen in Figure 5, the annual adjusted SRP values show the highest deviation from the SPP measurement. Even though the monthly adjusted SRP values were improved, the seasonal adjusted SRP (green) more significantly approached SPP measurement. To express this situation metrically, the averages of monthly differences between all the SRP values and SPP measurements given in Figure 5 were examined (Table 3).

In Table 3, the difference between SPP measurement and seasonal adjusted SRP is the lowest. Therefore, the seasonal coefficient was selected for SRP adjustment. The comparison of averages of yearly total values for calculated SRP, SPP measurement and adjusted SRP values were given in Table 4.

Table 3. The averages of monthly differences (kWh/m²).

Difference Between	Calculated SRP	Adjusted SRP		
		Monthly	Seasonal	Annual
SPP Meas. (2021-2022)	51.94	18.33	17.97	32.60

Table 4. The averages of the yearly total (kWh/m²).

	Calculated SRP	SPP Measurements	Adjusted SRP
2021-2022	1311.37	1934.66	1882.86

According to the averages of yearly total values given in Table 4, the difference between the calculated SRP and the SPP measurement values is approximately 46%. This difference decreases to 3% after the adjustment is applied. In this case, a 43% improvement was achieved by using AC. Thus, the seasonal AC was used to adjust the SRP values of roof patches. The seasonal adjusted total SRP for buildings is given in Figure 6.

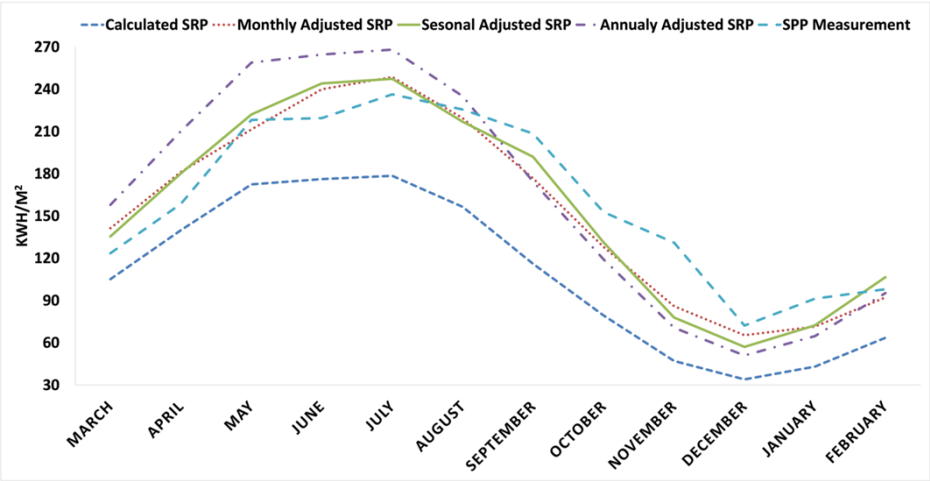

Figure 5. The comparison of monthly solar radiation average values.

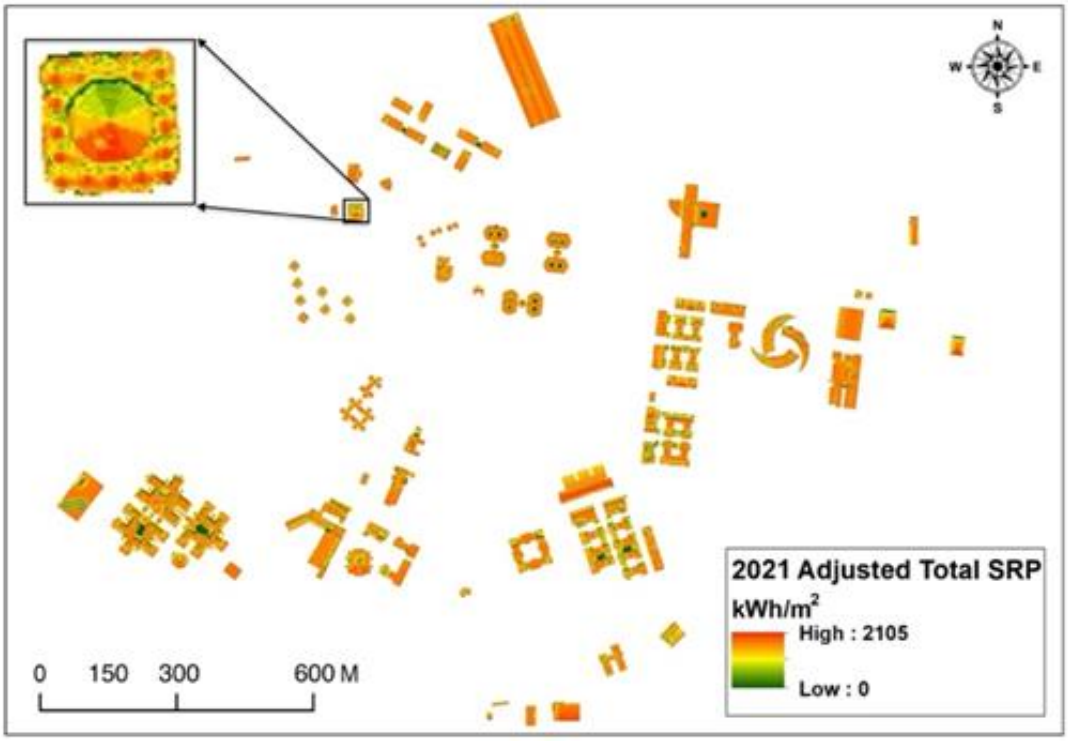

Figure 6. The adjusted total SRP for buildings.

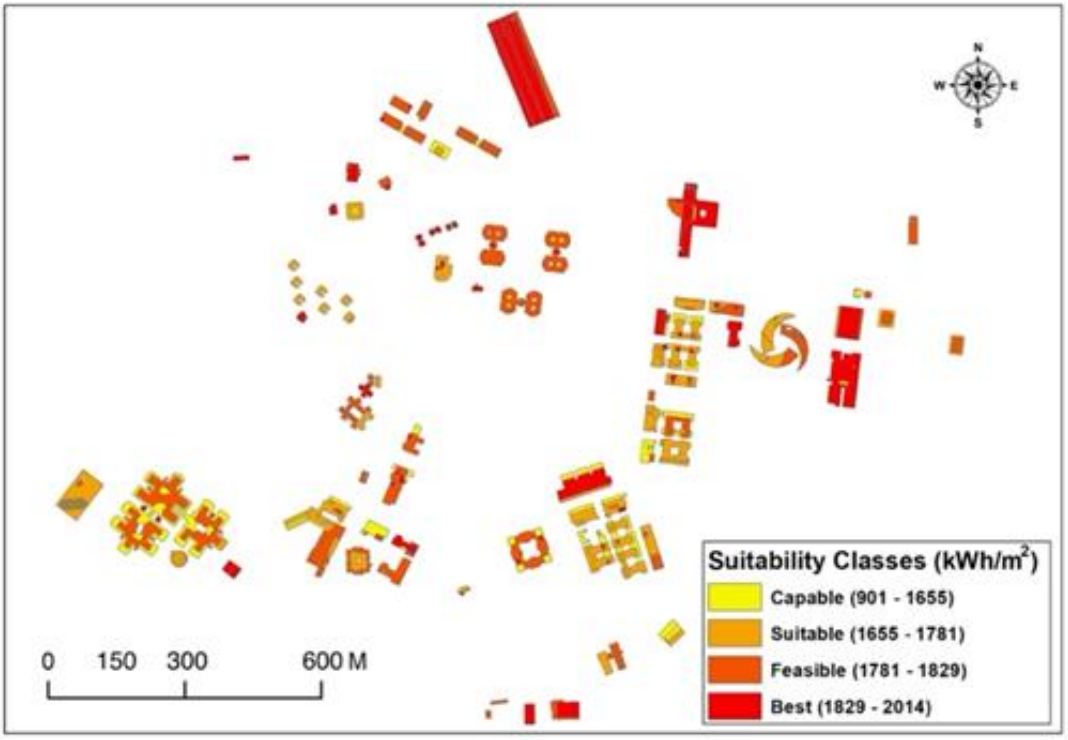

Figure 7. Suitability classes of roof patches for solar panel installation.

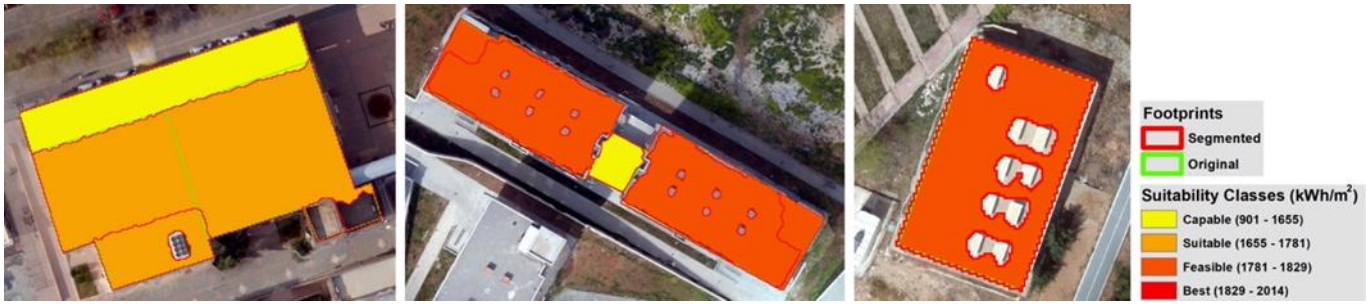

Figure 8. Suitability of the sample buildings.

In this study, 262 suitable roof patches were selected from all segmented parts regarding the parameters given in section 2.5. Also, a suitability classification was produced according to adjusted total SRP values to find the priority of the roof patches (Figure 7). Thus, flexibility has been provided in terms of which suitable roof patches should be preferred primarily in solar panel installation projects.

According to the results, the yearly SRP values for suitable patches varied from 901 to 2014 kWh/m^2 and the average SRP value of the whole suitable roof patches was calculated as 1715 kWh/m^2. The Capable class has the lowest area (13%) according to the whole suitable area. Similarly, the best class which has the highest SRP values covers 31% of the suitable area. In general, 87% of the suitable areas were highly efficient (yearly over 1655 kWh/m^2) for panel installation. A close view of the suitability of the sample buildings is given in Figure 8.

Rooftop segmentation and suitability classification provided detailed information for panel installation. For instance, when Figure 8 was examined, multiple suitability classes can be seen in an individual building due to the segmentation. Thus, it can be easily decided primarily on the installation patch for every building. Additionally, the unsuitable roof patches for solar panel installation were eliminated. It should be noted that the material for the construction of roofs is not investigated in the study. This situation needs to be considered in the installation process.

For further analysis, the adjusted SRP of usable roof patches was converted to the electricity potential. To achieve this, the same installation features of the SPP (25% tilt and 1.67 m^2 panel area) located in the study area were utilized. According to the panel manufacturer's 16% efficiency and 88% performance ratio values, the yearly theoretical electricity generation potential was calculated as 13 GWh. This calculated amount meets approximately 65% of campus consumption in 2021.

4. Conclusion

Today, traditional energy sources are declining, while energy demand is increasing. This trend is leading people to seek renewable energy sources. As a renewable energy source, solar energy has become more popular due to the wide range of accessibility from all around the world. At this point, the first step to establishing a facility is to determine SRP for the interested area. This process is easier for an open area, but it is complicated for rooftops. In this study, a workflow including photogrammetric UAV flight (DJI Mavic 2 Pro), SfM, image processing and GIS was used to detect both SRP and suitable roof patches for solar panel installation.

In the study, the UAV-based high-resolution DSM and SRP were generated for the study area. Then, three types of ACs were calculated based on long term SPP measurements. These ACs have been applied to the calculated values and compared with the 2021 measurements. Seasonal AC was chosen as it most closely approximates the GIS-based calculated values to the SPP measurements. This AC was used to adjust the SRP values of roof patches. To select suitable areas, the segmented roof patches and adjusted SRP were examined in consideration of the given installation parameters. Consequently, the selected roof patches were classified to find the priority of panel installation. According to the results, 87% of suitable roof patches were identified as highly efficient (yearly over 1655 kWh/m2) for solar panel installation. For a solid example, the adjusted SRP is converted to the electricity potential and compared with campus electricity consumption for 2021. It is seen that the potential of suitable roof patches corresponds to 65% of the actual electricity consumption for 2021.

It is necessary to visit each roof manually when UAV and GIS are not used to determine suitable areas for panel installation. In these manual visits, suitable areas for installation should be determined by considering the area of the roof, roof objects, and shadow areas. This is time consuming, costly, and labor-intensive when multiple buildings are involved. On the other hand, when UAV is used, roof areas and roof objects are obtained precisely, economically, and quickly, without making any building visits with high resolution orthophoto and DSM of the study area. In addition, the SRP values of the roofs that cannot be obtained by manual building visits can be calculated using GIS. In this way, suitable roof patches for panel installation and their priorities were determined. As a result, the UAV and GIS methods are more practical and effective than the manual method in terms of SRP calculation, data recording, time and personal safety, especially for local areas. Besides, the rooftop segmentation facilitates the detection of suitable areas for solar panel installation. In GIS-based SRP studies, values may deviate from the actual value due to multi-parametric algorithms. At this point, regional ACs may be used to correct the SRP values. In future studies, under which conditions and how much the AC value changes from region to region will be examined.

Acknowledgement

The authors would like to thank Harran University Renewable Energy Research Center (GAPYENEV) and Specialist M. Akif Ilkhan for providing data and their valuable contributions.

Author contributions

Nizar Polat: Conceptualization, Methodology, Software, Field study, Writing-Reviewing and Editing
Abdulkadir Memduhoğlu: Conceptualization, Methodology, Software, Field study, Writing-Reviewing and Editing

Conflicts of interest

The authors declare no conflicts of interest.

References

1. Ackermann, T. (2012). Wind power in power systems. John Wiley & Sons.
2. Chan, T. F., & Lai, L. L. (2007). An axial-flux permanent-magnet synchronous generator for a

direct-coupled wind-turbine system. IEEE Transactions on Energy Conversion, 22(1), 86-94. https://doi.org/10.1109/TEC.2006.889546

3. Elliott, D., Schwartz, M., Scott, G., Haymes, S., Heimiller, D., & George, R. (2003). Wind energy resource atlas of Sri Lanka and the Maldives (No. NREL/TP-500-34518). National Renewable Energy Lab. (NREL), Golden, CO (United States).
4. Bansal, R. C. (2003). Bibliography on the fuzzy set theory applications in power systems (1994-2001). IEEE Transactions on Power Systems, 18 (4) 1291-1299. https://doi.org/10.1109/TPWRS.2003.818595
5. Wang, Z., Bui, Q., Zhang, B., Nawarathna, C. L. K., & Mombeuil, C. (2021). The nexus between renewable energy consumption and human development in BRICS countries: The moderating role of public debt. Renewable Energy, 165, 381-390. https://doi.org/10.1016/j.renene.2020.10.144
6. Adjiski, V., Kaplan, G., & Mijalkovski, S. (2023). Assessment of the solar energy potential of rooftops using LiDAR datasets and GIS based approach. International Journal of Engineering and Geosciences, 8(2), 188-199. https://doi.org/10.26833/ijeg.1112274
7. Yılmaz, O. S., Gülgen, F., & Ateş, A. M. (2023). Determination of the appropriate zone on dam surface for floating photovoltaic system installation using RS and GISc technologies. International Journal of Engineering and Geosciences, 8(1), 63-75. https://doi.org/10.26833/ijeg.1052556
8. Demirgül, T., Demir, V., & Sevimli, M. F. (2023). Model-Ağacı (M5-tree) yaklaşımı ile HELIOSAT tabanlı güneş radyasyonu tahmini. Geomatik, 8(2), 124-135. https://doi.org/10.29128/geomatik.1137687
9. Arca, D., & Çıtıroğlu, H. K. (2022). Güneş enerjisi santral (GES) yapım yerlerinin CBS dayalı çok kriterli karar analizi ile belirlenmesi: Karabük Örneği, Geomatik, 7(1), 17-25. https://doi.org/10.29128/geomatik.803200
10. Choi, Y., Suh, J., & Kim, S. M. (2019). GIS-based solar radiation mapping, site evaluation, and potential assessment: A review. Applied Sciences, 9(9), 1960. https://doi.org/10.3390/app9091960
11. Nematollahi, O., & Kim, K. C. (2017). A feasibility study of solar energy in South Korea. Renewable and Sustainable Energy Reviews, 77, 566-579. https://doi.org/10.1016/j.rser.2017.03.132
12. Martín, A. M., Domínguez, J., & Amador, J. (2015). Applying LIDAR datasets and GIS based model to evaluate solar potential over roofs: a review. Aims Energy, 3(3), 326-343. https://doi.org/10.3934/energy.2015.3.326
13. Yalcin, M., Dereli, M. A., & Ugur, M. A. (2019). Modeling of solar energy potential with geographical information system and remote sensing integration: A case study for Bergama, Turkey. International Symposium on Applied Geoinformatics (ISAG-2019), 136–164.
14. Huang, Y., Chen, Z., Wu, B., Chen, L., Mao, W., Zhao, F., ... & Yu, B. (2015). Estimating roof solar energy potential in the downtown area using a GPU-accelerated solar radiation model and airborne LiDAR data. Remote Sensing, 7(12), 17212-17233. https://doi.org/10.3390/rs71215877
15. Kucuksari, S., Khaleghi, A. M., Hamidi, M., Zhang, Y., Szidarovszky, F., Bayraksan, G., & Son, Y. J. (2014). An Integrated GIS, optimization and simulation framework for optimal PV size and location in campus area environments. Applied Energy, 113, 1601-1613. https://doi.org/10.1016/j.apenergy.2013.09.002
16. Verso, A., Martin, A., Amador, J., & Dominguez, J. (2015). GIS-based method to evaluate the photovoltaic potential in the urban environments: The particular case of Miraflores de la Sierra. Solar Energy, 117, 236-245. https://doi.org/10.1016/j.solener.2015.04.018
17. Polat, N., & Uysal, M. (2018). An experimental analysis of digital elevation models generated with Lidar Data and UAV photogrammetry. Journal of the Indian Society of Remote Sensing, 46(7), 1135-1142. https://doi.org/10.1007/s12524-018-0760-8
18. Toprak, A. S., Polat, N., & Uysal, M. (2019). 3D modeling of lion tombstones with UAV photogrammetry: a case study in ancient Phrygia (Turkey). Archaeological and Anthropological Sciences, 11(5), 1973-1976. https://doi.org/10.1007/s12520-018-0649-z
19. Uysal, M., Toprak, A. S., & Polat, N. (2015). DEM generation with UAV Photogrammetry and accuracy analysis in Sahitler hill. Measurement, 73, 539-543. https://doi.org/10.1016/j.measurement.2015.06.010
20. Polat, N., & Uysal, M. (2017). DTM generation with UAV based photogrammetric point cloud. The International Archives of the Photogrammetry, Remote Sensing and Spatial Information Sciences, 42, 77-79. https://doi.org/10.5194/isprs-archives-XLII-4-W6-77-2017
21. Shao, H., Song, P., Mu, B., Tian, G., Chen, Q., He, R., & Kim, G. (2021). Assessing city-scale green roof development potential using Unmanned Aerial Vehicle (UAV) imagery. Urban Forestry & Urban Greening, 57, 126954. https://doi.org/10.1016/j.ufug.2020.126954
22. Dewanto, B. G., Novitasari, D., Tan, Y. C., Puruhito, D. D., Fikriyadi, Z. A., & Aliyah, F. (2020). Application of web 3D GIS to display urban model and solar energy analysis using the unmanned aerial vehicle (UAV) data (Case study: National Cheng Kung university buildings). IOP Conference Series: Earth and Environmental Science, 520(1), 012017. https://doi.org/10.1088/1755-1315/520/1/012017
23. Fuentes, J. E., Moya, F. D., & Montoya, O. D. (2020). Method for estimating solar energy potential based on photogrammetry from unmanned aerial vehicles. Electronics, 9(12), 2144. https://doi.org/10.3390/electronics9122144
24. Turkish State Meteorological Service (2021). Turkish State Meteorological Service. https://mgm.gov.tr/kurumici/turkiye-guneslenme-suresi.aspx

25. Global Solar Atlas (2021). Global Solar Atlas. https://globalsolaratlas.info/map?c=37.68382,36.112061,6.
26. Rich, P., Dubayah, R., Hetrick, W., & Saving, S. (1994). Using viewshed models to calculate intercepted solar radiation: applications in ecology. American Society for Photogrammetry and Remote Sensing Technical Papers. American Society of Photogrammetry and Remote Sensing, 524-529.
27. Fu, P., & Rich, P. M. (2002). A geometric solar radiation model with applications in agriculture and forestry. Computers and Electronics in Agriculture, 37(1-3), 25-35. https://doi.org/10.1016/S0168-1699(02)00115-1
28. Kırcalı, Ş., & Selim, S. (2021). Site suitability analysis for solar farms using the geographic information system and multi-criteria decision analysis: the case of Antalya, Turkey. Clean Technologies and Environmental Policy, 23, 1233-1250. https://doi.org/10.1007/s10098-020-02018-3
29. Nelson, J. R., & Grubesic, T. H. (2020). The use of LiDAR versus unmanned aerial systems (UAS) to assess rooftop solar energy potential. Sustainable Cities and Society, 61, 102353. https://doi.org/10.1016/j.scs.2020.102353
30. Snavely, N., Seitz, S. M., & Szeliski, R. (2008). Modeling the world from internet photo collections. International Journal of Computer Vision, 80, 189-210. https://doi.org/10.1007/s11263-007-0107-3
31. Lucieer, A., Turner, D., King, D. H., & Robinson, S. A. (2014). Using an Unmanned Aerial Vehicle (UAV) to capture micro-topography of Antarctic moss beds. International Journal of Applied Earth Observation and Geoinformation, 27, 53-62. https://doi.org/10.1016/j.jag.2013.05.011
32. Li, B., Xu, X., Zhang, L., Han, J., Bian, C., Li, G., ... & Jin, L. (2020). Above-ground biomass estimation and yield prediction in potato by using UAV-based RGB and hyperspectral imaging. ISPRS Journal of Photogrammetry and Remote Sensing, 162, 161-172. https://doi.org/10.1016/j.isprsjprs.2020.02.013
33. Yang, H., Hu, X., Zhao, J., & Hu, Y. (2021). Feature extraction of cotton plant height based on DSM difference method. International Journal of Precision Agricultural Aviation, 4(1), 59-69. https://doi.org/10.33440/j.ijpaa.20210401.151
34. Boonpook, W., Tan, Y., & Xu, B. (2021). Deep learning-based multi-feature semantic segmentation in building extraction from images of UAV photogrammetry. International Journal of Remote Sensing, 42(1), 1-19. https://doi.org/10.1080/01431161.2020.1788742
35. Haralick, R. M., Shanmugam, K., & Dinstein, I. H. (1973). Textural features for image classification. IEEE Transactions on Systems, Man, and Cybernetics, (6), 610-621. https://doi.org/10.1109/TSMC.1973.4309314
36. Šúri, M., & Hofierka, J. (2004). A new GIS-based solar radiation model and its application to photovoltaic assessments. Transactions in GIS, 8(2), 175-190. https://doi.org/10.1111/j.1467-9671.2004.00174.x
37. ESRI (2021). Modeling solar radiation. https://pro.arcgis.com/en/pro-app/latest/tool-reference/spatial-analyst/modeling-solar-radiation.htm
38. ESRI (2021). How solar radiation is calculated. https://pro.arcgis.com/en/pro-app/latest/tool-reference/spatial-analyst/how-solar-radiation-is-calculated.htm
39. Fu, P. (2000). A geometric solar radiation model with applications in landscape ecology. [Doctoral dissertation, University of Kansas].
40. Fröhlich, C., & Brusa, R. W. (1981). Physikalisch-meteorologisches observatoriurn, world radiation center, davos, switzerland. Sol Physics, 74, 16-19.
41. Khanna, D. (2020). Estimate solar power potential. In: Learn ArcGIS. https://learn.arcgis.com/en/projects/estimate-solar-power-potential/#
42. Palmer, D., Koumpli, E., Cole, I., Gottschalg, R., & Betts, T. (2018). A GIS-based method for identification of wide area rooftop suitability for minimum size PV systems using LiDAR data and photogrammetry. Energies, 11(12), 3506. https://doi.org/10.3390/en11123506
43. Yang, Y., Campana, P. E., Stridh, B., & Yan, J. (2020). Potential analysis of roof-mounted solar photovoltaics in Sweden. Applied Energy, 279, 115786. https://doi.org/10.1016/j.apenergy.2020.115786
44. Zhong, Q., & Tong, D. (2020). Spatial layout optimization for solar photovoltaic (PV) panel installation. Renewable Energy, 150, 1-11. https://doi.org/10.1016/j.renene.2019.12.099